Synthesis and Crystal Structure Determination of a New Pressure-Induced Iridium Ditelluride Phase, *m*-$IrTe_2$, and Comparison of the Crystal Structures and Relative Stabilities of Various $IrTe_2$ Polymorphs

S. Jobic,[†] R. Brec,*[,‡] C. Chateau,[‡] J. Haines,[‡] J.-M. Léger,[‡] H.-J. Koo,[§] and M.-H. Whangbo*[,§]

Institut des Matériaux Jean Rouxel, 2 rue de la Houssinière, BP 32229, 44322 Nantes Cedex 3, France, Laboratoire de Physico-Chimie des Matériaux, CNRS, 1 place Aristide Briand, 92190 Meudon, France, and Department of Chemistry, North Carolina State University, Raleigh, North Carolina 27695-8204

Received April 4, 2000

The new monoclinic $IrTe_2$ phase *m*-$IrTe_2$ was synthesized under pressure, and its structure was determined by X-ray powder diffraction. The relative stabilities of the three known and three hypothetical $IrTe_2$ polymorphs were discussed on the basis of tight binding electronic band structure calculations. *m*-$IrTe_2$ exhibits structural features of both CdI_2^- and pyrite-type $IrTe_2$ phases and is expected to be nearly as stable as that of the CdI_2-type $IrTe_2$. The hypothetical IrS_2- and ramsdellite-type $IrTe_2$ phases are predicted to be more stable than the CdI_2-type $IrTe_2$.

1. Introduction

The ability of tellurium to possess a wide range of Te−Te bonding and nonbonding contact distances is an important factor to consider in understanding the structural and physical properties of transition-metal tellurides.[1−6] These compounds exhibit Te···Te distances ranging from the Te−Te single bond length of $(Te_2)^{2-}$ dimers (∼2.75 Å), to medium bonding lengths as in $IrTe_2$ ($Te^{1.5-}$−$Te^{1.5-}$ ≈ 3.53 Å), and to the Te^{2-}···Te^{2-} nonbonding van der Waals contact distance (∼4.0 Å). The oxidizing power of the chalcogen decreases in the order S > Se > Te, and this raises the p-block band energy of Te with respect to that of S or Se. Thus, in tellurides, the filled 5p-block bands of the tellurium anions may overlap with the empty or partially filled d-block bands of the transition-metal cations, hence causing electron transfer from the 5p-block to the d-block bands. Since the top portion of the 5p-block bands is antibonding between Te atoms, the electron depletion from these bands decreases the overlap repulsion between the Te···Te contacts, thereby decreasing their distances. This phenomenon may even induce partial and extended bonding between the anions, giving rise to "polymeric short bonding contacts" [1,2] within the tellurium anion sublattice. Due to the diffuseness of the valence 5s/5p orbitals of Te, the overlap between Te atoms falls off gradually as the Te−Te distance is increased. This explains the diversity of Te−Te bonding and nonbonding contact distances found for tellurides.

It is possible to alter slightly the nature (bonding/nonbonding) of the Te···Te contacts in tellurides by changing the transition metal and hence modifying the energies and occupancies of the d-block levels. The same can be achieved by physical means. For instance, an external pressure will shorten the Te···Te distances and hence raise the top portion of the 5p-block band levels, which then induces electron transfer from the 5p band to the lower-lying transition-metal d levels. The latter leads to a new charge balance and may cause structural modifications. Indeed, when a sample of the polymeric CdI_2-type $IrTe_2$ (hereafter referred to as *h*-$IrTe_2$ because of its hexagonal cell) is subjected to pressure up to 32 GPa at room temperature, two new forms of $IrTe_2$ are obtained.[7] The first structural transition takes place around 5 GPa and leads to a monoclinic form (hereafter referred to as *m*-$IrTe_2$). The second transition, which occurs at 20 GPa and room temperature, gives rise to the cubic pyrite-type $IrTe_2$ (hereafter referred to as *c*-$IrTe_2$) reported earlier.[7]

In the present work, we describe the crystal structure of *m*-$IrTe_2$, which is isolated as a pure, well-crystallized compound at 750 °C and 4.5 GPa. We then compare the crystal structures of the *h*-, *m*-, and *c*-$IrTe_2$ phases and investigate their relative stabilities and charge balances on the basis of extended Hückel tight binding (EHTB) electronic band structure calculations.[8,9] Finally we discuss the possibility of obtaining other polymorphs of $IrTe_2$ by performing EHTB calculations on hypothetical structures. The atomic orbital parameters employed for our calculations were taken from the previous studies.[3,4]

2. Experimental Section

Polymeric CdI_2-type $IrTe_2$ powder[10] (∼67 mg) was precompacted into a pellet (3.0 mm in diameter and 1.1 mm in height) at ∼0.4 GPa in a WC die. The pellet was then treated at 750 °C under 4.5 GPa for

[†] Institut des Matériaux Jean Rouxel.
[‡] CNRS.
[§] North Carolina State University.

(1) Jobic, S.; Brec, R.; Rouxel, J. *J. Alloys Compds.* **1992**, *178*, 253.
(2) Rouxel, J. *Comments Inorg. Chem.* **1992**, *14*, 207.
(3) Canadell, E.; Jobic, S.; Brec, R.; Rouxel, J.; Whangbo, M.-H. *J. Solid State Chem.* **1992**, *96*, 189.
(4) Whangbo, M.-H.; Canadell, E. *J. Am. Chem. Soc.* **1992**, *114*, 9587.
(5) Alemany, P.; Jobic, S.; Brec, R.; Canadell, E. *Inorg. Chem.* **1997**, *36*, 5050.
(6) Sheldrick, W. S.; Wachhold, M.; Jobic, S.; Brec, R.; Canadell, E. *Adv. Mater.* **1997**, *9*, 669.
(7) Léger, J.-M.; Pereira, A. S.; Haines, J.; Jobic, S.; Brec, R. *J. Phys. Chem. Solid* **2000**, *61*, 27.
(8) Whangbo, M.-H.; Hoffmann, R. *J. Am. Chem. Soc.* **1978**, *100*, 6397.
(9) Our calculations were carried out by employing the CAESAR program package (Ren, J.; Liang, W.; Whangbo, M.-H. *Crystal and Electronic Structure Analysis Using CAESAR*, 1998; this book can be downloaded free of charge from the Web site http://www. PrimeC.com/.).
(10) Jobic, S.; Deniard, P.; Brec, R.; Rouxel, J. *Z. Anorg. Allg. Chem.* **1991**, *598/599*, 199.

10.1021/ic000351e CCC: $19.00
Published on Web 08/30/2000

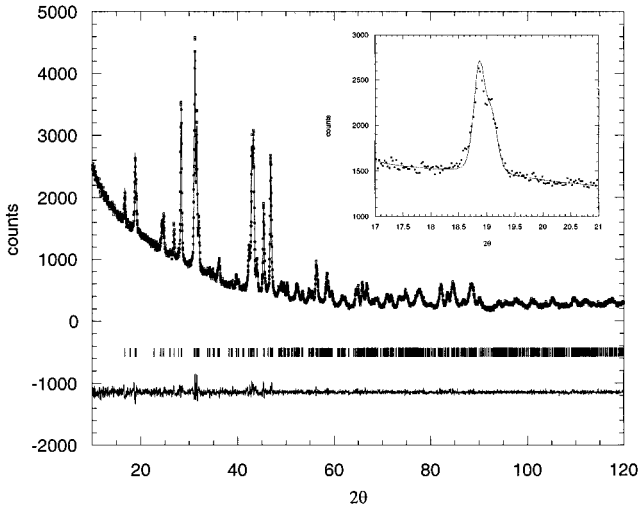

Figure 1. Rietveld refinement of the diffraction data recorded for *m*-$IrTe_2$ on a Siemens D5000 diffractometer with a Bragg−Brentano geometry. The calculated (—) and observed (···) profiles are shown at the top, and the difference between the two is shown at the bottom. The inset emphasizes the separation of the $20\bar{1}$ peaks (at 18.796° and 18.843°) from the 201 peaks (at 19.022° and 19.069°).

4.5 h in a high-pressure apparatus of a belt type. The sample was thermally quenched (T < 100 °C after 10 s)[11] and, after slow decompression, was ground and analyzed by X-ray powder diffraction.

Black powder samples (M_r = 447.42) were sieved at 50 μm and then dispersed on a silica plate with acetone to prevent preferential orientation. Diffraction data were collected by using a Siemens D5000 diffractometer without a monochromator (Cu Kα1, 1.540 598 Å, Cu Kα2, 1.544 390 Å; reflection geometry; linear counter with a 2 deg/min sweep speed; 2θ range = 10−120°). The digitization of the powder pattern was carried out with a 0.03° step. It was not possible to assign the diffraction peaks to any known material, so we conclude that our synthesis leads to monophasic samples. An automatic indexing of the X-ray pattern was successfully run with the Dicvol91 package.[12] A full pattern matching analysis (Fullprof)[13] of the X-ray pattern of 733 reflections, including a pseudo-Voigt and Caglioti description of the peak shapes and half-width, was carried out. The background was manually subtracted by cubic spline interpolation between points. This led to the following crystal data: space group monoclinic $C2/m$ (no. 12), a = 19.975(1) Å, b = 4.0016(2) Å, c = 5.3119(3) Å, β = 90.818(3)°, V = 424.54(4) Å^3, Z = 6, and ρ_{calcd} = 10.500 g/cm^3. The correctness of $\beta \neq 90°$ was confirmed using highly resolved diffraction data recorded in a Debye−Scherrer geometry on an INEL CPS 120 position-sensitive detector with a 2θ range of 0−120° (Cu Kα1 radiation and $Na_2Ca_3Al_2F_{14}$ as standard). This ruled out the possibility of an orthorhombic cell. For instance, the examination of the X-ray pattern in the 2θ range between 19° and 21° evidenced two well-separated peaks at 18.796° and 19.022°. These correspond to the $20\bar{1}$ and 201 diffraction planes, respectively, and confirm that the symmetry of the unit cell is monoclinic. The peak split is less marked on the Siemens D5000 pattern due to the presence of the Cu Kα1 and Cu Kα2 radiations but is clearly visible as presented in the inset of Figure 1. Although the use of the monochromatized INEL device provides a better distinction between diffraction peaks, the structure refinement was carried out using the data obtained with a nonmonochromatic radiation to avoid the problem of a large absorption in a Debye−Scherrer configuration.

The structure refinement of the X-ray powder pattern was performed using the Rietveld method, and the atomic positions were determined by the direct method using the Expo code.[14] The resulting positional and thermal parameters of the Ir and Te atoms are listed in Table 1.

Table 1. Fractional Coordinates and Thermal Parameters of the Ir and Te Atoms of the *m*-$IrTe_2$ Phase

atom	x	y	z	B (Å^2)
Ir(1)	0.3398(2)	0.0	0.0027(7)	0.29(8)
Ir(2)	0.5	0.5	0.5	0.3(1)
Te(1)	0.4556(3)	0.0	0.7754(8)	0.7(1)
Te(2)	0.2809(2)	0.5	0.7545(8)	0.6(1)
Te(3)	0.3804(2)	0.5	0.2802(8)	0.7(1)

The final reliability factors are R_p = 3.99%, R_{wp} = 5.50%, R_{exp} = 3.87%, and χ^2 = 2.02. The possibility of texture was tested by refining the preferential orientation with a March function, but no improvement of refinement was observed. An overview of the refinement fit is given in Figure 1.

3. Results and Discussion

A. Crystal Structure. The structural building blocks of *m*-$IrTe_2$ are $IrTe_6$ octahedra. A schematic projection view of the crystal structure of *m*-$IrTe_2$ in the *ac* plane is presented in Figure 2, where the $IrTe_6$ octahedra share edges and corners. It should be noted that the *h*-$IrTe_2$ phase has only edge-sharing $IrTe_6$ octahedra, and the *c*-$IrTe_2$ only corner-sharing $IrTe_6$ octahedra.

m-$IrTe_2$ can be viewed as constructed by sharing the corners of $[Ir(1)_2Te_6]_\infty$ double rutile chains and $[Ir(2)Te_4]_\infty$ single rutile chains running along the *b* direction. Alternatively, *m*-$IrTe_2$ can be viewed as an ordered intergrowth of the ramsdellite and pyrolusite layers[15] in the 1:1 ratio in the *a* direction. In the γ-MnO_2 structure[15] the ramsdellite and pyrolusite layers stack randomly. *m*-$IrTe_2$ can also be considered as a derivative of the IrS_2 structure type,[16,17] in which the ramsdellite and pyrolusite layers occur in the 1:2 ratio in an ordered manner.

The Ir−Te distances and cis Te−Ir−Te bond angles of the $IrTe_6$ octahedra in *m*-$IrTe_2$ are comparable to those in the *h*- and *c*-$IrTe_2$ phases[7,10] under ambient conditions. The short interoctahedral Te−Te distances found for *m*-$IrTe_2$ are Te(1)−Te(1) = 2.953(7) Å and Te(2)−Te(3) = 3.231(6) Å (the thick solid and dashed lines in Figure 2, respectively). The Te(1)−Te(1) distance is slightly shorter than that of the $(Te_2)^{2-}$ dimers (3.075 Å) in *c*-$IrTe_2$ at 0.1 GPa.[7] Each Te(1)−Te(1) unit should be regarded as a $(Te_2)^{2-}$ dimer. However, each Te(2)−Te(3) unit cannot be considered as a $(Te_2)^{2-}$ dimer, although it is considerably shorter in length than the short interoctahedral Te−Te distance of *h*-$IrTe_2$ (3.497 Å)[10] under ambient conditions.

B. Electronic Structure. The plots of the electronic density of states (DOS) calculated for the *h*-, *m*-, and *c*-$IrTe_2$ phases at 0.1 GPa using the EHTB method are presented in Figure 3. The solid lines refer to the total DOS curves, the dotted lines to the partial DOS curves for the Ir 5d orbitals, and the vertical dashed lines to the Fermi levels. Calculations indicate that the *m*-$IrTe_2$ phase is slightly less stable than the *h*-$IrTe_2$ phase (ΔE = 2.2 kcal/mol per formula unit), while the *c*-$IrTe_2$ phase is considerably less stable than the *h*-$IrTe_2$ phase (ΔE = 25 kcal/mol per formula unit). Moreover, the Fermi levels (i.e., the highest occupied energy levels) increase in the order *h*-$IrTe_2$ (−10.7 eV) < *m*-$IrTe_2$ (−9.1 eV) < *c*-$IrTe_2$ (−8.5 eV). This trend reflects the fact that the extent of antibonding in the Te·

(11) Chateau, C.; Haines, J.; Léger, J. M.; Lesauze, A.; Marchand, R. *Am. Mineral.* **1999**, *84*, 207.
(12) Boultif, A.; Louër, D. *J. Appl. Crystallogr.* **1991**, *24*, 987.
(13) Rodriguez-Carjaval, J. *Physica B* **1993**, *19*, 55.
(14) Altomare, A.; Burla, M. C.; Cascarano, G.; Giocovazzo, C.; Guargliardi, A.; Moliterni, A. G. G.; Polidori, G. *J. Appl. Crystallogr.* **1995**, *28*, 842.
(15) Wells, A. F. *Structural Inorganic Chemistry*; Oxford University Press: Oxford, U.K., 1962.
(16) Barricelli, L. B. *Acta Crystallogr.* **1958**, *11*, 75.
(17) Jobic, S.; Deniard, P.; Brec, R.; Rouxel, J.; Drew, M. G. B.; David, W. I. F. *J. Solid State Chem.* **1990**, *89*, 315.

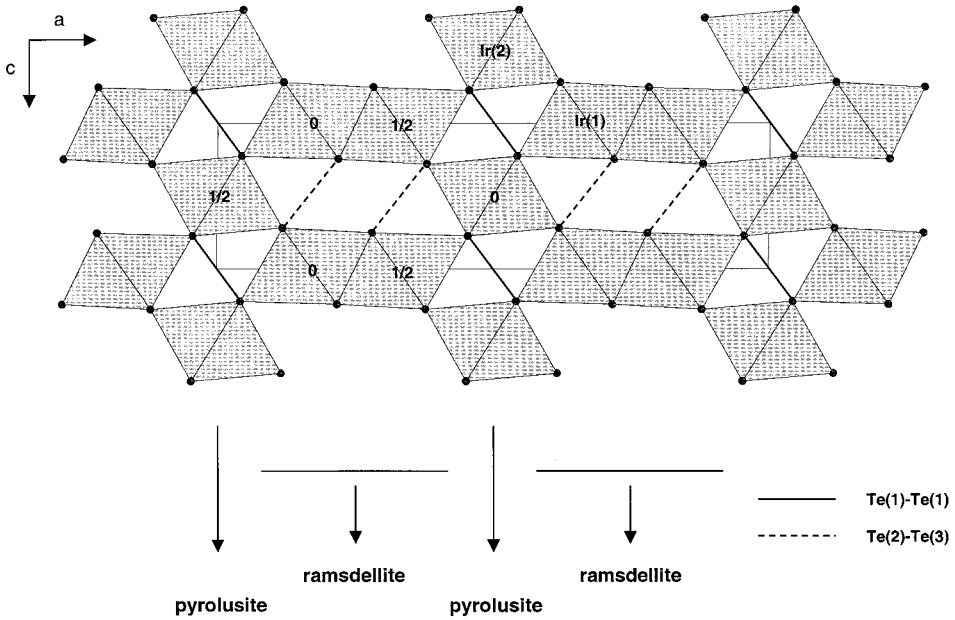

Figure 2. Schematic projection view of *m*-$IrTe_2$ along the *b* axis, where the rectangle represents a unit cell, and each shaded rhombus represents an $IrTe_6$ octahedron. The thick solid and dashed lines between $IrTe_6$ octahedra refer to the interoctahedral Te(1)−Te(1) (2.953 Å) and Te(2)−Te(3) (3.231 Å) contacts, respectively. Selected bond lengths (Å) are Ir(1)−Te(1) = 2.625(7), Ir(1)−Te(2) = 2.661(4) (×2), Ir(1)−Te(2) = 2.750(6), Ir(1)−Te(3) = 2.608(4) (×2), Ir(2)−Te(1) = 2.640(3) (×4), and Ir(2)−Te(3) = 2.644(4) (×2).

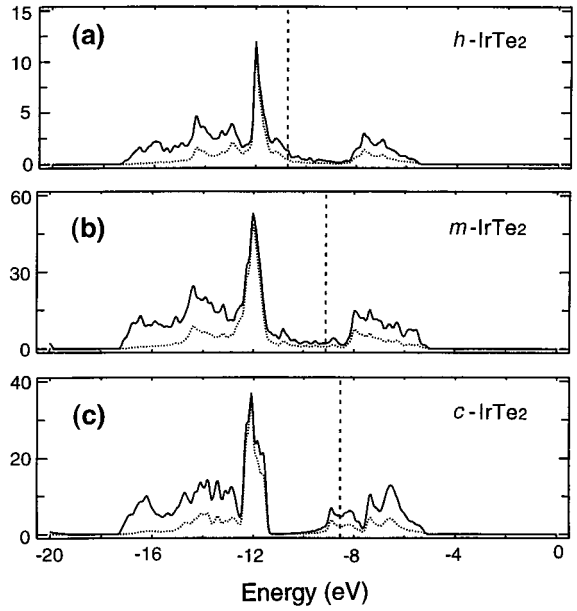

Figure 3. DOS plots calculated for the crystal structures of (a) *h*-$IrTe_2$ at 0.1 GPa, (b) *m*-$IrTe_2$ at 0.1 GPa, and (c) *c*-$IrTe_2$ at 0.1 GPa. The solid curves refer to the total DOS curves, the dotted curves to the partial DOS curves of the Ir 5d orbitals, and the vertical dashed lines to the Fermi levels. The units on the vertical axes are in electrons per unit cell. The unit cells of the *h*-, *m*-, and *c*-$IrTe_2$ phases have one, six, and four formula units, respectively.

··Te interactions around the Fermi level increases in the order *h*-$IrTe_2$ < *m*-$IrTe_2$ < *c*-$IrTe_2$.

We also carried out electronic band structure calculations for the 32 GPa structures of *h*-$IrTe_2$ and *c*-$IrTe_2$.[7] As expected, these calculations show that the *h*-$IrTe_2$ and *c*-$IrTe_2$ phases are less stable at 32 GPa than at 0.1 GPa. The gross populations calculated for the Ir atoms reveal that, as the pressure increases from 0.1 to 32 GPa, each Ir atom of *h*-$IrTe_2$ gains about 0.42 electron, and each Ir atom of *c*-$IrTe_2$ gains about 0.15 electron. (The pressure-induced Te → Ir electron transfer is less pronounced in the pyrite phase since iridium has a lower oxidation state in *c*-$IrTe_2$ than in *h*-$IrTe_2$ in ambient conditions, as will be discussed below). Thus, a pressure increase raises the 5p-block band levels of Te more than the 5d-block levels of Ir, thus leading to an oxidation of the Te anion.

C. Charge Balance. To a first approximation, the charge balance for *h*-$IrTe_2$ may be written as $(Ir^{3+})(Te^{1.5-})_2$ considering the stability of the $Ir^{3+}(d^6)$ low-spin configuration.[1,10] This formulation implies a sizable separation between the t_{2g}- and e_g-block bands of Ir as well as the presence of an empty e_g-block band of Ir and a partially filled 5p-block band of the Te anions. This picture is consistent with the DOS plot of *h*-$IrTe_2$ shown in Figure 3a. Due to the stability of the $Ir^{3+}(d^6)$ low-spin configuration and the presence of one $(Te_2)^{2-}$ dimer per three formula units in *m*-$IrTe_2$, the charge balance for *m*-$IrTe_2$ may be written as $(Ir^{3+})_3(Te_2)^{2-}(Te^{1.75-})_4$. Here the possibility of a mixed valence Ir^{3+}/Ir^{2+} in *m*-$IrTe_2$ was ruled out, because the gross populations of the nonequivalent Ir atoms are calculated to be nearly the same (the gross population of Ir(1) is larger than that of Ir(2) by 0.18 electron). The reduction of Ir^{3+} into Ir^{2+} in *c*-$IrTe_2$ gives rise to the charge balance $Ir^{2+}(Te_2)^{2-}$ with a partial occupation of the e_g-block bands (see Figure 3c). Thus, as summarized in Figure 4, an external pressure on *h*-$IrTe_2$ first causes the charge disproportionation, $3Te^{1.5-} \rightarrow Te^{1-} + 2Te^{1.75-}$, leading to *m*-$IrTe_2$ and then the reduction of Ir^{3+} into Ir^{2+} and a complete dimerization of tellurium, giving rise to *c*-$IrTe_2$.

D. Other Possible Phases. So far, the IrS_2-, ramsdellite-, and pyrolusite-type $IrTe_2$ phases have not been synthesized. To examine the feasibility of preparing such phases, we construct their probable structures and evaluate their relative stabilities. As mentioned in section 3.A, the Ir−Te bonds and the intraoctahedral Te···Te distances do not depend much on the structure types. Therefore, we build the hypothetical structures of the IrS_2-, ramsdellite-, and pyrolusite-type $IrTe_2$ phases on the basis of the crystal structures of $IrSe_2$,[16,17] ramsdellite MnO_2,[18] and pyrolusite MnO_2,[19] respectively, by keeping

(18) Bystroem, A. M. *Acta Chem. Scand.* **1949**, *3*, 163.
(19) Baur, W. H. *Acta Crystallogr. B* **1976**, *32*, 2200.

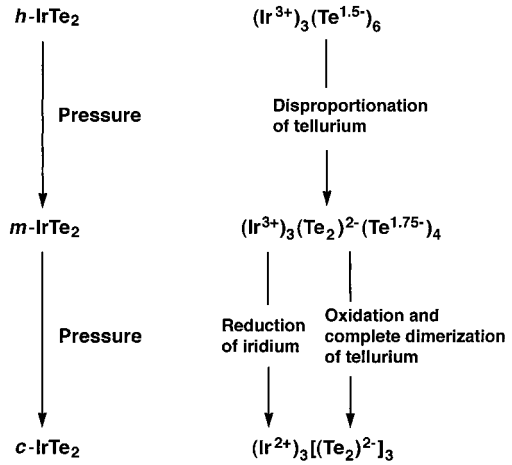

Figure 4. Pressure-induced change in the charge balance of the three $IrTe_2$ polymorphs.

constant the fractional coordinates of the atoms but by uniformly increasing the cell parameters (i.e., 0.070%, 0.398%, and 0.405%, respectively) so that the average of the resulting Ir−Te distances becomes 2.650 Å as found in the three known $IrTe_2$ polymorphs under ambient conditions. Our EHTB electronic band structure calculations for these hypothetical structures suggest that the IrS_2-type $IrTe_2$ is considerably more stable than *h*-$IrTe_2$ ($\Delta E = -18$ kcal/mol), and the ramsdellite-type $IrTe_2$ is slightly more stable than *h*-$IrTe_2$ ($\Delta E = -1.5$ kcal/mol). However, the pyrolusite-type $IrTe_2$ is considerably less stable than *h*-$IrTe_2$ ($\Delta E = 11$ kcal/mol). It would be interesting to see if the IrS_2- or ramsdellite-type $IrTe_2$ phases can be synthesized.

To check the reliability of the relative energies of the $IrTe_2$ polymorphs discussed in the present work, we also carried out first-principles electronic band structure calculations for various $IrTe_2$ polymorphs using the VASP program[20,21] package. These calculations[22] support the main conclusions of the present EHTB calculations that *m*-$IrTe_2$ is nearly as stable as *h*-$IrTe_2$, but the *c*-$IrTe_2$ phase is considerably less stable than *h*-$IrTe_2$, and that the hypothetical IrS_2- and ramsdellite-type $IrTe_2$ phases are more stable than *h*-$IrTe_2$, but the hypothetical pyrolusite-type $IrTe_2$ is considerably less stable than *h*-$IrTe_2$. The first-principles calculations suggest that *m*-$IrTe_2$ is slightly more stable than *h*-$IrTe_2$.

4. Concluding Remarks

The *m*-$IrTe_2$ phase prepared under pressure is made up of edge- and corner-sharing $IrTe_6$ octahedra, whereas the *h*- and *c*-$IrTe_2$ phases have only edge- and corner-sharing $IrTe_6$ octahedra, respectively. It is expected that *m*-$IrTe_2$ is nearly as stable as *h*-$IrTe_2$, but considerably more stable than *c*-$IrTe_2$. The *h*-$IrTe_2$ → *m*-$IrTe_2$ phase transition induces the Te charge disproportionation, $3Te^{1.5-} \rightarrow Te^{1-} + 2Te^{1.75-}$, while the *m*-$IrTe_2$ → the *c*-$IrTe_2$ phase transition causes a Te → Ir electron transfer and a complete $(Te_2)^{2-}$ dimer formation. Preparation of the hypothetical ramsdellite- and IrS_2-type $IrTe_2$ phases appears feasible, but that of the pyrolusite-type $IrTe_2$ phase does not.

Acknowledgment. The work at North Carolina State University was supported by the Office of Basic Energy Sciences, Division of Materials Sciences, U.S. Department of Energy, under Grant DE-FG05-86ER45259.

IC000351E

(20) Kresse, G.; Hafner, J. *Phys. Rev. B* **1993**, *47*, 558.
(21) Kresse, G. Thesis, Technische Universität Wien, 1993.
(22) Jobic, S.; Brec, R.; Pasturel, A.; Koo, H.-J.; Whangbo, M.-H. Manuscript in preparation.